Motion-adapted catheter navigation with real-time instantiation and improved visualisation

Article *in* Journal of Robotic Surgery · September 2013
DOI: 10.1007/s11701-013-0423-2

7 authors, including:

Su-Lin Lee
Imperial College London
63 PUBLICATIONS **377** CITATIONS
SEE PROFILE

Ka-Wai Kwok
The University of Hong Kong
52 PUBLICATIONS **537** CITATIONS
SEE PROFILE

Colin D Bicknell
Imperial College London
131 PUBLICATIONS **1,510** CITATIONS
SEE PROFILE

Nick Cheshire
Imperial College London
223 PUBLICATIONS **4,142** CITATIONS
SEE PROFILE

J Robotic Surg (2013) 7:251–260
DOI 10.1007/s11701-013-0423-2

SPECIAL ISSUE: HAMLYN SYMPOSIUM 2012

Motion-adapted catheter navigation with real-time instantiation and improved visualisation

Su-Lin Lee · Ka-Wai Kwok · Lichao Wang · Celia Riga · Colin Bicknell · Nicholas Cheshire · Guang-Zhong Yang

Received: 31 January 2013 / Accepted: 15 July 2013 / Published online: 25 July 2013

Abstract The improvements to catheter manipulation by the use of robot-assisted catheter navigation for endovascular procedures include increased precision, stability of motion and operator comfort. However, navigation through the vasculature under fluoroscopic guidance is still challenging, mostly due to physiological motion and when tortuous vessels are involved. In this paper, we propose a motion-adaptive catheter navigation scheme based on shape modelling to compensate for these dynamic effects, permitting predictive and dynamic navigations. This allows for timed manipulations synchronised with the vascular motion. The technical contribution of the paper includes the following two aspects. Firstly, a dynamic shape modelling and real-time instantiation scheme based on sparse data obtained intra-operatively is proposed for improved visualisation of the 3D vasculature during endovascular intervention. Secondly, a reconstructed frontal view from the catheter tip using the derived dynamic model is used as an interventional aid to user guidance. To demonstrate the practical value of the proposed framework, a simulated aortic branch cannulation procedure is used with detailed user validation to demonstrate the improvement in navigation quality and efficiency.

Keywords Robotic surgery · Minimally invasive surgery · Endovascular intervention · Image-guided intervention · Shape modelling · Motion prediction

S.-L. Lee (✉) · K.-W. Kwok · L. Wang · G.-Z. Yang
Hamlyn Centre for Robotic Surgery, Imperial College London, London SW7 2AZ, UK
e-mail: su-lin.lee@imperial.ac.uk

C. Riga · C. Bicknell · N. Cheshire
Academic Division of Surgery, Imperial College London, London, UK

Introduction

The manipulation of catheters through complex anatomy has undergone improved consistency and safety through the introduction of robotic catheter navigation systems such as the Hansen Magellan (Hansen Medical, Mountain View, CA, USA) for arterial intervention [1] and the Stereotaxis Niobe (Stereotaxis, St. Louis, MO, USA) for electrophysiology (EP) procedures [2]. The use of these systems has led to greater stability of the catheter, as well as better control, allowing for catheter manoeuvrability though more tortuous vessels. Furthermore, the benefits of robotic guidance include the potential for better operator ergonomics, a reduction in radiation exposure, a reduction in procedure time and a reduction in embolisation risk to the patient [3].

There are several technical hurdles to be overcome, however, before the full benefits of robot assistance in minimally invasive endovascular procedures can be realised. One such hurdle is the imaging modality currently used for guidance; X-ray fluoroscopy provides a 2D projection of the 3D scene and is unable to show the boundaries of the vessels without the use of an iodine contrast agent, of which the use is strongly controlled due to its nephrotoxicity. In addition, errors in navigation, for example during stent graft placement, can result in potential damage to the vessel walls which may result in dissection, embolization or subsequent neointimal hyperplasia. Likewise, incorrect stent placement may increase the risk of stent migration or excessive pressure may lead to blood vessel rupture, with dire consequences.

Most current commercial systems are able to integrate models or point clouds generated from pre-operative data for intra-operative guidance, using co-registration of what is often a static 3D vasculature; these are uninformative

when applied to complex procedures, such as deploying branched and fenestrated stent grafts, in regions where the vasculature is affected by motion and deformation. Anatomical co-registration and localisation of dynamic details have been greatly simplified by recent advances in intra-operative imaging such as combined X-ray radiography/magnetic resonance (XMR) and computed tomography fluoroscopy (fluoro-CT). Although they can provide detailed 3D coverage during endovascular procedures, pulse-programming constraints or nephrotoxicity and ionising radiation concerns limit their practical use for real-time continuous 3D imaging. Clinically, it is therefore more desirable to use sparse data coverage intra-operatively combined with shape or dynamic information obtained pre-operatively to instantiate the full 3D shape.

In image-guided intervention, an ongoing research topic has been the prediction of respiratory and cardiac motion, required for intra-operative motion synchronisation and adaptation. To this end, methods based on 3D model-based registration [4, 5] and predictive adaptation during image-guided intervention [6] have been developed. With aortic branch cannulation, there is a chance of aortic dissection or plaque dislodgement, risking possible stroke, if the robotic catheter is not advanced with care through the dynamic vasculature—there is a particular risk of cerebral embolisation during endovascular procedures in the aortic arch [7]. The aortic arch and its branches are affected by the cardiac cycle through two mechanisms: firstly, the proximity of the aorta to the myocardium during contraction and, secondly, the haemodynamic effects caused by the pulsatile blood flow. This can affect the path plan for the catheters, as seen in Fig. 1. While it is possible to map an ideal path based on the centreline of an angiography roadmap, each roadmap is only obtained at one point in time and does not take into account the dynamics of the vessel.

In addition, non-rigid vascular shift may also be induced by the introduction of a guidewire or catheter during an endovascular procedure [8]. Likewise, the presence of stent grafts, stiff wires and stent delivery devices introduce additional vessel deformation. To ensure safety, consistency and efficiency of the procedure, timed manipulations (e.g. for cannulation around bifurcations) synchronised with vascular motion and deformation is required and predictive dynamic modelling would aid in compensating for the dynamics of the vasculature.

However, the use of a dynamic model alone will not solve all guidance problems; the method of presentation of this extra data to the clinician is vital. There have been investigations into the use of a generated, virtual endoscopic visualisation, a method of visualisation through a 3D image volume or model, for endovascular guidance. The use of virtual endoscopy was originally derived from 3D volumes obtained pre-operatively and used for surgical planning and simulation. Deschamps and Cohen [9], for example, defined a method of extracting a path suitable for virtual endoscopy directly from 3D images. Virtual endoscopy has been investigated for many applications, including neurosurgery [10], interventional pulmonology [11], and interventional cardiology [12].

Currently, most commercial imaging systems for the angiography suite (e.g. dyna-CT systems) include a method of automatically generating a virtual endoscopic flythrough from a contrast-enhanced CT scan of the vasculature. However, for intra-operative use, these systems are limited to overlaying a static 3D model derived from a CT angiography onto the X-ray fluoroscopy for guidance. Sun et al. [12, 13] investigated the use of virtual endoscopy to visualise the coronary artery plaques for diagnostic purposes. From initial results, they

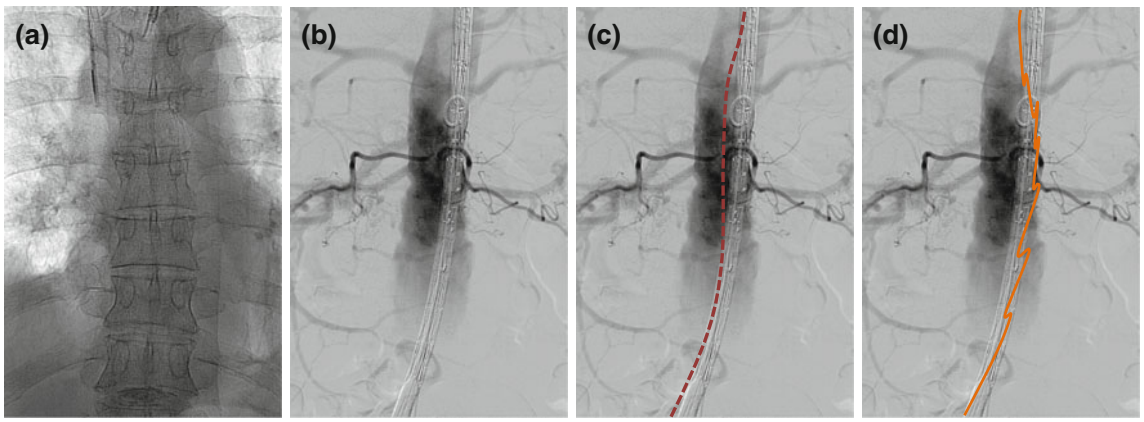

Fig. 1 An example of the X-ray images seen during an endovascular procedure: **a** with no contrast, the soft tissue and vessels cannot be seen. **b** With contrast agent, a roadmap of the vessels (here the aorta) is produced. **c** The optimal path (*red*) for the catheter to travel can be displayed on this roadmap but (**d**) in reality, the motion of the catheter (*orange*) is affected by motion, such as respiration and the cardiac cycle

demonstrated the potential of the visualisation to show the intraluminal configuration of plaques but only compared the virtual endoscopy to 2D axial images. Wang et al. [14] proposed a method of placing a catheter within complex vascular anatomy using an electromagnetic system to track the catheter within a model derived from CT angiography. This would provide continuous virtual visual feedback to the operator during a minimally invasive procedure. However, while the proposed method is promising, the evaluation of its use intra-operatively is limited.

The aim of this paper is to propose a model-guided framework for improved endovascular guidance and navigation. First, an effective shape modelling and real-time model guidance scheme based on dynamic shape instantiation is introduced; sparse data is collected during the procedure and is couple with prior data to generate models for improved visualisation of the 3D arterial roadmap. Second, a reconstructed frontal view from the catheter tip is implemented using the dynamic model and is demonstrated on a simulated aortic branch cannulation procedure with detailed user validation, showing how the derived dynamic model can be used to improve navigation quality and efficiency during an endovascular procedure.

Methods

Predictive motion modelling and real-time instantiation

The predictive motion model proposed in this work was based on previous development on a dynamic shape instantiation framework [15]. A statistical shape model (SSM) of the vasculature (in this study, the aortic arch) is first built; this requires a training set of 3D shapes of the anatomy of interest and the SSM describes the range of motion or morphology within this training set. A SSM can be built group-wise or on a subject-specific basis. As the aortic arch is complex and there are variations in the arrangement of the aortic branches arising from the arch across subjects, a subject-specific model is more appropriate. A number of landmarks were obtained on the hemi-diaphragm on the imaging data for each phase of the respiratory cycle. The positions of the landmarks obtained and their corresponding 3D models of the aortic arch were used to train the dynamic shape instantiation. Other respiratory positions obtained can then be used as further input to the shape instantiation to determine their corresponding 3D models.

The dynamic shape instantiation is based on partial least squares regression (PLSR):

$$\hat{Y} = XB_{\mathrm{PLS}}$$

$$B_{\mathrm{PLS}} = \left(P^{T+}\right)DQ^{T}$$

where the calculation of the new outputs is only a matrix multiplication with the new inputs. The new inputs X will be predicted respiratory positions and they will be multiplied by matrix B_{PLS} to generate new output (a set of vertices defining a 3D mesh) $\hat{Y}$. D is the matrix with the regression weights on the diagonal, P is the loading matrix on X, Q is the loading matrix on Y, and P^{T+} is the pseudoinverse of the transpose of P.

With PLSR, instead of determining the relationship between inputs and outputs directly on the variables themselves, the variables are first projected onto new axes, reducing the dimensionality of the set. As the number of faces and numbering of the faces will not change (this is set in the corresponding mesh files used in the training set), only the new vertex positions are determined by the output.

A Kalman filter [16] was introduced to predict and correct the positions of the respiratory cycle across time. The diaphragm positions measured from the MR images are z_k and these are used to update the Kalman filter for each state k:

$$\hat{x}_k = \hat{x}_{\bar{k}} + K_k\left(z_k - H\hat{x}_{\bar{k}}\right)$$

where K is the Kalman gain, H is the matrix relating the state to the measurements z_k, and $\hat{x}_k$ and $\hat{x}_{\bar{k}}$ are the state estimate and a priori state estimate, respectively. An input stream of respiratory positions was used, with the filter correcting and updating the estimates of the current state of respiration. The predicted meshes were then used as input to the dynamic shape instantiation to obtain the complete 3D mesh of the aortic arch at that respiratory position. Overall, the limited data, in the form of the respiratory positions, obtained intra-operatively are used to generate the full 3D shape using knowledge trained from pre-operatively obtained data. An overview of the proposed technique is shown in Fig. 2.

Data acquisition

Patient data

To build the SSM for the shape instantiation model, a set of 3D volume imaging data was required. Eight normal subjects (four male and four female) were scanned on a Siemens Avanto 1.5T scanner at the Royal Brompton Hospital in London and MR images of the ascending and descending aortas were collected. A series (approximately 50 images in total) of single-shot coronal images covering the entire lung field were acquired using a steady state free precession sequence (TR = 2.8 ms, TE = 1.2 ms, asymmetric echo,

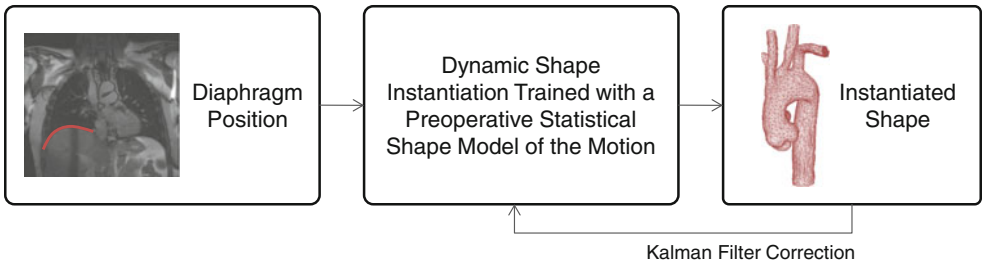

Fig. 2 A summary of the predictive motion modelling based on dynamic shape instantiation

in-plane resolution = 1.6 × 1.6 mm, slice thickness = 4 mm, slice separation = 0.8 mm). The scans were cardiac gated with the imaging performed in diastole.

The subjects were free breathing during this scan and a novel respiratory feedback system was used to avoid changes in the breathing cycle for the duration of the scan. An MR navigator was used to determine the location of the dome of the right hemi-diaphragm and this were recorded immediately before and after the acquisition of each coronal image. These were also recorded into a text file for the timings of each slice to be determined subsequently for retrospective volume reconstruction. To cover a number of positions in the respiratory cycle, the multi-slice coronal acquisitions were repeated 40 times.

The navigator positions were displayed to the subject being scanned via a strip of LED lights—multiple green lights bounded by yellow lights and finally red lights. This encouraged the subject to keep their breathing constant and within the green "safe" area. This imaging sequence and LED board was originally developed for imaging of the lungs [17].

The aortic arches and brachiocephalic arteries were segmented from the DICOM images and meshed, using Analyze (AnalyzeDirect, Inc., Overland Park, KS, USA). The set of arches made up the training set for a statistical shape model that was used in the prediction motion model. For each arch, correspondence was achieved by rigidly registering the reference shape to each shape in the model and projecting the reference points to the surface. This ensured that each shape in the training set had an equal number of points and that the same points corresponded to the same anatomical landmarks. An example of the patient data is shown in Fig. 3.

The mean errors of the predicted models were calculated, with errors calculated as the Euclidean distance from each mesh node to its corresponding node in the other mesh.

Phantom data

For the SSM for the user evaluation of the dynamic model and the reconstructed frontal view, a set of image volumes of a dynamic phantom data set was acquired. A silicone phantom of an aortic arch by Elastrat Sàrl (Geneva, Switzerland) was CT scanned in a GE Innova 4100 interventional X-ray machine. The phantom was scanned five times at five different dynamic positions; each position was obtained by a varying number of inserts placed next to the ascending aorta to mimic the motion the aorta undergoes during respiration. As before, the structure was segmented and meshed with the Analyze software and processed as described above.

The number of inserts was used in place of respiratory positions in the prediction motion model built using the meshed data as input. A respiratory cycle was set at 4 s long and the meshes along this cycle were predicted using diaphragm positions determined using the equation by Lujan et al. [18]. A leave-one-out study was performed for each of the five predicted meshes and the mean errors were calculated for each of them.

User evaluation with reconstructed frontal view

An experiment was set up to assess the effect of visualising the shape-instantiated prediction of the aorta dynamics when performing a simulated cannulation. The silicone phantom meshes derived from the predictive motion model were used in conjunction with an estimated kinematic model of a tendon-wire-based robotic catheter. These kinematics are generalised as a control mapping from the manual input degrees of freedom (DoFs) to the movement along the image plane of the reconstructed frontal view. The catheter is steerable by two pairs of tendons attached along the catheter, each coupled with an actuator that drives the catheter in bidirectional bending [19]. The catheter can be considered as a flexible continuum robot; however, in reality, the kinematics are complicated by respiration, cardiac contraction, pulsatile blood flow, catheter flexibility and even the length of the catheter advanced inside the vasculature. With the aim of evaluating the effect of the reconstructed frontal view (simulating the placement of a camera at the catheter tip, similar to a virtual endoscopic view or fly's eye view) with dynamic shape modelling, but not involving other

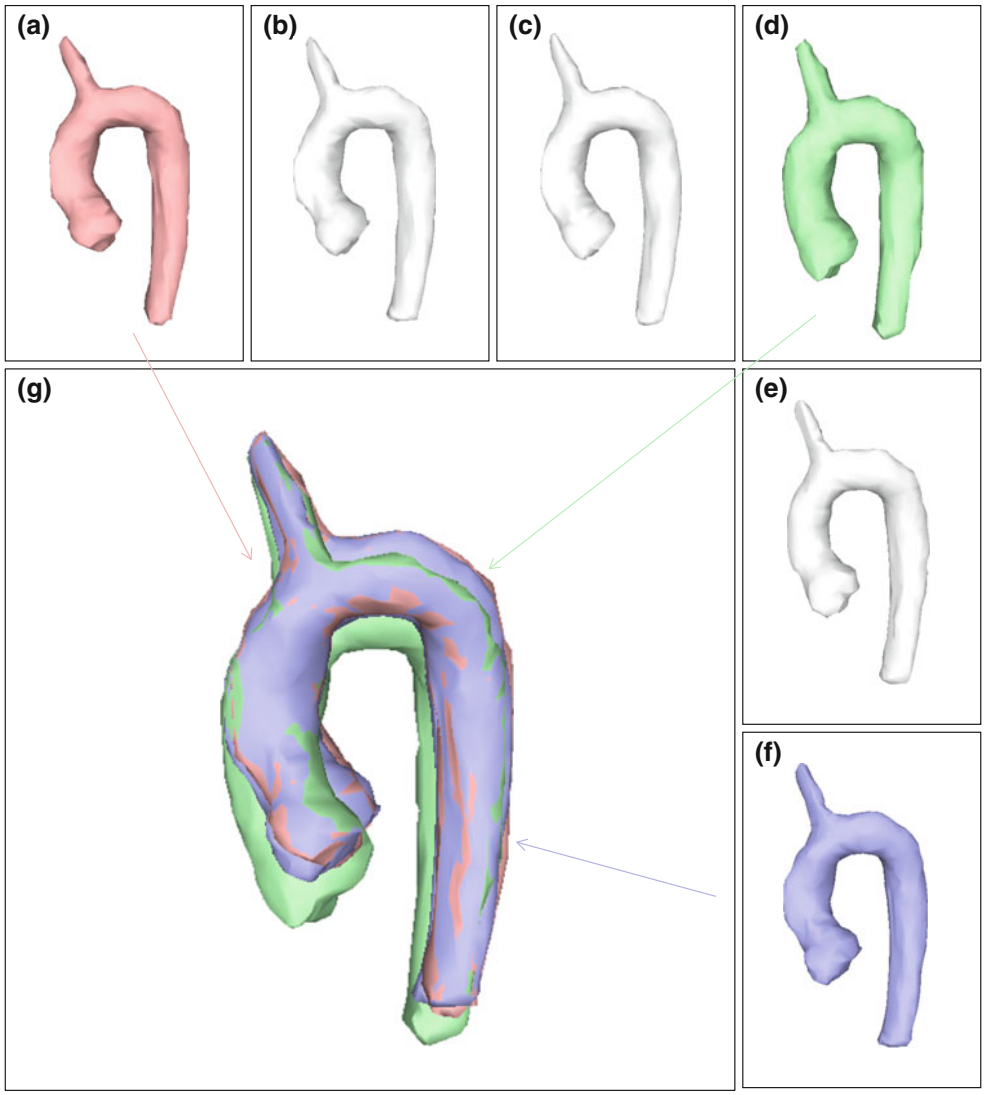

Fig. 3 An example of the patient data collected: **a–f** the meshes from one subject across the respiratory cycle and **g** selected meshes overlaid on each other, highlighting the motion in the aortic arch caused by respiration

complications like the aforementioned variation of catheter kinematics, in this simulation, we therefore attempt to stabilise the control kinematic mapping which enables the operator to coordinate the manipulation relative to the vasculature. For instance, the operator can navigate the catheter with the correct alignment between the visual and motor axes [20].

Detailed assessment of the use of the predicted motion model to aid in timed manipulation through deforming bifurcations is possible using this simulation environment. With the availability of a predicted motion model of the vasculature and the position of the robotic catheter known at all times, a reconstructed frontal view was also generated, allowing the operator to 'drive' the catheter through the vessels with this view simulating a camera on the catheter tip.

Nine operators (all right-hand dominant, all novice users with no endovascular intervention experience but with experience of using video game inputs, mean age 27.2 ± 3.6 years) were recruited to assess the proposed technique. These operators were to cannulate the left subclavian artery (LSA) in the vascular mesh using the model of the robotic catheter. The catheter was controlled by a PHANTOM Omni haptic device (SensAble Tech. Inc., USA) to simulate the remote control similar to that available on a Hansen Sensei/Magellan. The user evaluation setup is shown in Fig. 4. Figure 4a shows the silicone phantom used, Fig. 4b gives three views of the predicted motion model and the simulated robotic catheter during one experiment, and Fig. 4c shows the corresponding reconstructed frontal views from the catheter at the positions in Fig. 4b.

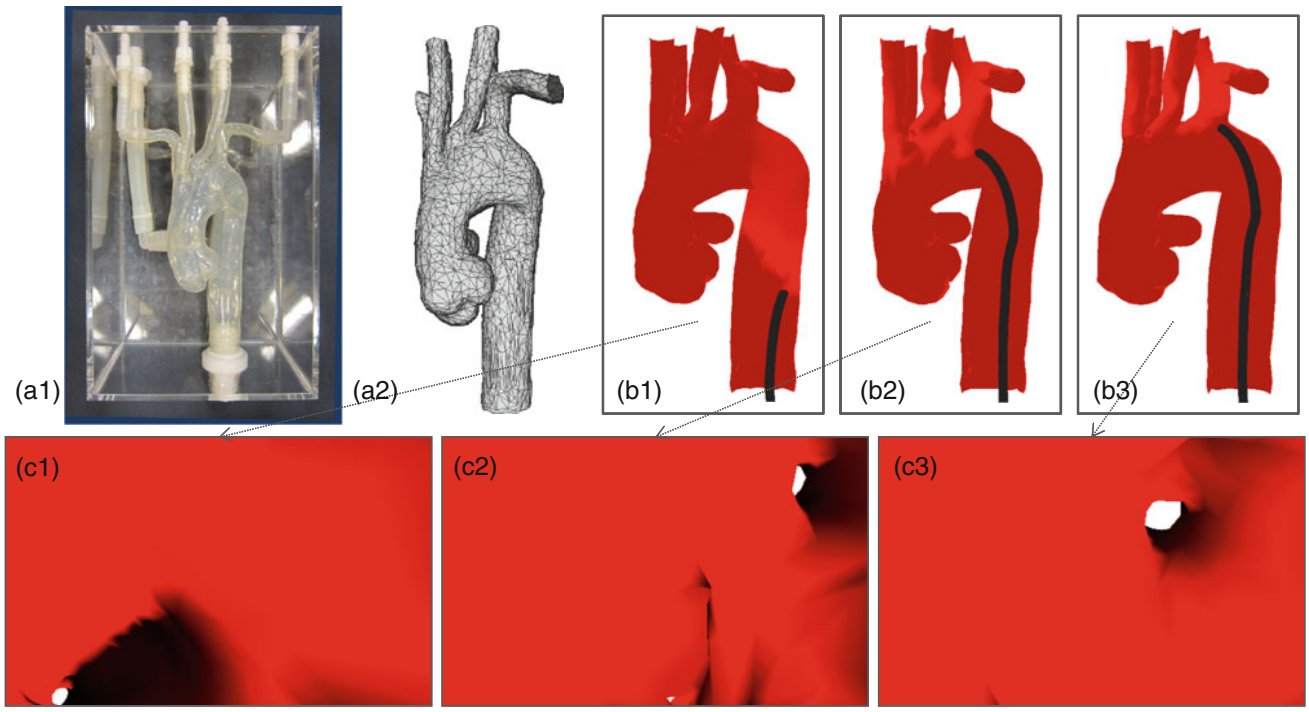

Fig. 4 The setup of the user evaluation experiments: **a** the silicone phantom and one of the meshes generated from it, **b** three frames of the predicted motion model and the simulated robotic catheter, and **c** the corresponding reconstructed frontal views from the catheter tip

All the experiments were performed on the same desktop PC and each operator performed the procedure twice, with and without the reconstructed frontal view. The phantom visualisation was initialised to the plane of the aortic arch, the view most used by clinicians when performing an endovascular intervention under X-ray fluoroscopy, and the subject operators were allowed to adjust the orientation of the vascular mesh during the procedure. In order to remove any bias caused by the learning effect, the order in which the experiments were performed was randomised. Prior to the experiment, the operators were allowed approximately 5 min to familiarise themselves with the control of the catheter and were well advised of the clinical risks of making wall contact with the catheter tip.

A number of performance indices were recorded or derived from the available data and are shown in Table 1.

The indices chosen include those quantitative metrics used in clinical studies [21] and the others make use of the known positions of the simulated robotic catheter tip and model over time. The last two metrics relate to the way in which the operators manipulate the robotic catheter.

The Euclidean distance from the catheter tip to the closest point on the surface of the current mesh was calculated at each time point. A collision was recorded when the catheter tip distance to the mesh was 0.001 mm. The optimal path was defined by the centreline of the mesh obtained using the mesh thinning algorithm implemented by Thinvox [22].

Table 1 The performance indices recorded or derived in the experiments

Performance indices
Total number of catheter tip-mesh collisions
Total duration when the catheter tip is along the mesh walls
Completion time
Total path length of the catheter tip
Mean deviation of the catheter tip from the optimal path
Total number of operator pauses during the procedure
Total number of distinct operator manipulations during the procedure

To assess the differences between procedures performed with and without the reconstructed frontal view, a Kruskal–Wallis non-parametric test was used.

Results

The range of errors for the leave-one-out validation on the phantom data is shown in Fig. 5b. Figure 5a shows the range of errors across the respiratory cycle for each subject scanned. Overall, most of the errors are within a few millimetres; the large errors in Subject 7 may be due to misregistration during data acquisition.

Table 2 shows the performance indices recorded across all nine operators for the use of the dynamic model and

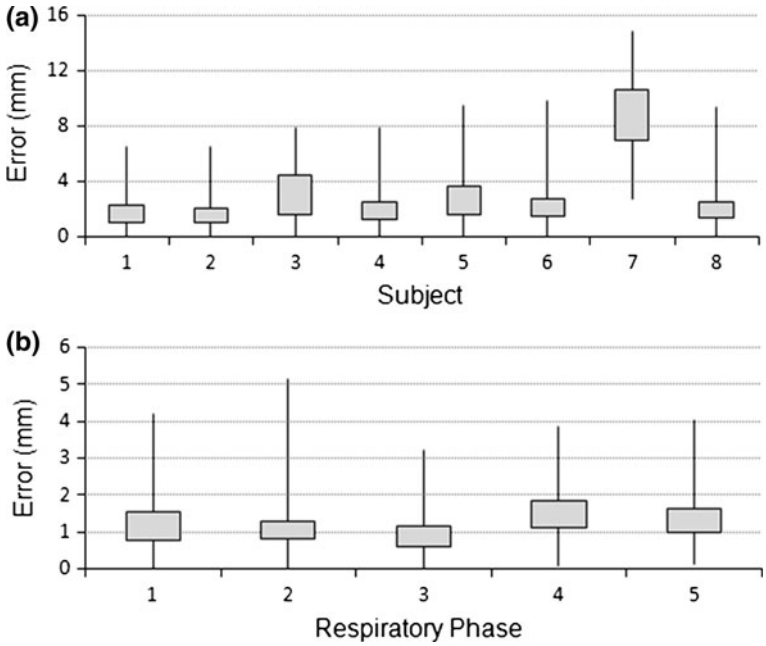

Fig. 5 Box and whisker plots (showing the median, minimum, maximum and first and third quantiles of the data) for the data across **a** the leave-one-out study of the respiratory cycles of the eight subjects scanned and **b** the leave-one-out study of the dynamic silicone phantom

with and without the use of the reconstructed frontal view; the means and standard deviations of each index are shown both with and without the reconstructed frontal view. It can be seen that most of the performance metrics improved significantly during cannulation of the LSA using the reconstructed frontal view and the proposed dynamic shape model. For the first five metrics, the results are statistically significant (Kruskal–Wallis; $p < 0.05$). The last two metrics concerning robotic catheter manipulation did not have statistically significant differences between the two experiments.

The number of mesh collisions and the duration of time the catheter tip was against the vessel wall have both reduced, suggesting improved safety of cannulation by reducing the risk of vessel dissection. All the operators made comments on how the reconstructed frontal view made the procedure easier and none required reorientation of the 3D dynamic model when using the reconstructed frontal view.

Detailed performance results for three operators are displayed in Fig. 6. Figure 6a shows one subject (Operator 4) whose performance improved the most using the reconstructed frontal view along with the dynamic motion model while Fig. 6c shows the subject (Operator 9) whose performance remained the same. Figure 6b (Operator 6) shows the improvement that occurs across the majority of the operators in the experiment. With the reconstructed frontal view, the catheter tip path is smoother and the procedure time and mean deviation of the centreline decreased. Across all operators, the paths cover a smaller region (or remain the same) and are mostly smoother with the use of both the dynamic model and the reconstructed frontal view. Overall, these results suggest safer and more efficient catheterisation.

Discussion

Overall, the metrics show improvement in catheter navigation with the use of the dynamic shape model and the reconstructed frontal view. The hypothesis we intended to test in this study is that the use of the reconstructed frontal view may affect the way in which the operators handled the robotic catheter. The main metrics were greatly improved: completion time, the overall path length, the mean deviation from the ideal path, the number of mesh collisions, and the duration the catheter tip spent against the vessel walls were reduced. We had also expected the operators to advance the catheter with more confidence and longer insertion strokes. However, the results suggest that, even with this new visualisation scheme, operators still handle the catheter carefully to prevent accidents. The two metrics for this (total number of operator pauses during procedure and total number of distinct operator manipulations during procedure) show no statistically significant differences between the experiments with and without the reconstructed frontal view.

Currently, the models used to train the shape instantiation are obtained pre-operatively. While the method allows for some flexibility in predicting shapes outside the range defined by the training set, large deformations caused by interaction between the catheter or guidewire or stent

Table 2 The performance indices of the nine operators cannulating the LSA with the dynamic model with and without (in parentheses) the reconstructed frontal view

Metric	Operator										
	1	2	3	4	5	6	7	8	9	Mean	Standard deviation
Completion time (s)	59.9 (107.0)	96.9 (61.44)	142.5 (130.87)	28.6 (194.2)	79.8 (105.0)	48.6 (62.5)	100.3 (158.3)	48.0 (87.3)	41.1 (63.5)	71.8 (107.8)	36.3 (46.3)
Path length (mm)	326.1 (524.9)	587.5 (527.9)	643.7 (992.8)	262.9 (2,564.2)	446.8 (808.9)	255.3 (541.3)	313.8 (600.0)	258.0 (697.7)	460.5 (688.0)	395.0 (882.9)	147.0 (648.8)
Path deviation (mm)	5.8 (9.7)	6.3 (8.1)	6.9 (12.4)	5.3 (18.5)	5.7 (15.3)	6.4 (9.9)	6.4 (6.9)	4.3 (10.7)	5.1 (6.2)	5.8 (10.9)	0.8 (4.0)
No. of mesh collisions	2 (1)	0 (6)	1 (0)	0 (32)	0 (11)	1 (9)	1 (5)	0 (5)	7 (7)	1.3 (8.4)	2.2 (9.5)
Duration along walls (s)	1.3 (1.5)	0.0 (6.5)	0.1 (0.0)	0.0 (5.4)	0.0 (3.0)	0.4 (10.8)	0.9 (1.9)	0.0 (6.7)	2.6 (2.4)	0.6 (4.2)	0.9 (3.4)
No. times catheter stopped	29 (21)	27 (55)	46 (52)	74 (13)	36 (28)	30 (31)	37 (32)	24 (24)	30 (32)	37.0 (32.0)	15.3 (13.7)
No. times catheter manipulated	12 (8)	10 (18)	25 (24)	40 (6)	18 (15)	14 (12)	18 (16)	13 (12)	14 (13)	18.2 (13.8)	9.3 (5.4)

delivery devices with the vessel walls cannot be predicted. Online biomechanical modelling would enhance the current framework [23] but increase the computation time. With the incorporation of GPU processing [24], it may be possible to calculate deformations in real-time, but this is still in the research stage.

In this study, we have used a haptic device to simulate the remote control device for a robotic catheter. While this is a popular control interface for prototype robotic devices, it does not perfectly simulate the control currently available on control systems. For example, the Hansen Magellan system offers both remote catheter manipulator as well as a set of arrow keys, similar to that on a conventional computer keyboard. Other robotic catheter devices use different means of control: the Stereotaxis Niobe uses mouse input while the Amigo system [25] uses a remote control that mimics the normal steerable EP catheter control. Investigation of methods by which to simulate this control is also proposed.

Future work planned also includes the incorporation of the model with dynamic active constraints [26] which would allow for online determination of catheter tip proximity to the dynamic model and hence provide real-time haptic feedback to the operator. Dynamic pathways can be defined for robotic catheter navigation, giving clear benefits over static roadmaps. Safety margins, including a distance tolerance to the centreline, can be prescribed prior to the intervention and such feedback can prevent the operator from venturing to the riskier regions. For endovascular interventions, the method is foreseen to be particularly needed at locations where there is large motion; one example is for cannulation of the renal arteries for infra-renal stent placement, where there is much respiratory motion due to their proximity to the diaphragm.

Conclusion

A motion-adapted catheter navigation scheme with dynamic shape modelling and real-time instantiation is presented. The proposed framework is able to instantiate shapes outside the provided training set and thus is suitable for the use of a predictive motion model for intra-operative navigation.

The use of a reconstructed frontal view from the catheter tip along with the dynamic model was employed in a user evaluation for intra-operative endovascular navigation. Detailed results have shown that the combination of the dynamic model of the vasculature and reconstructed frontal view can facilitate adaptive path planning and timed synchronisation, leading to increased overall safety and consistency of intervention procedures.

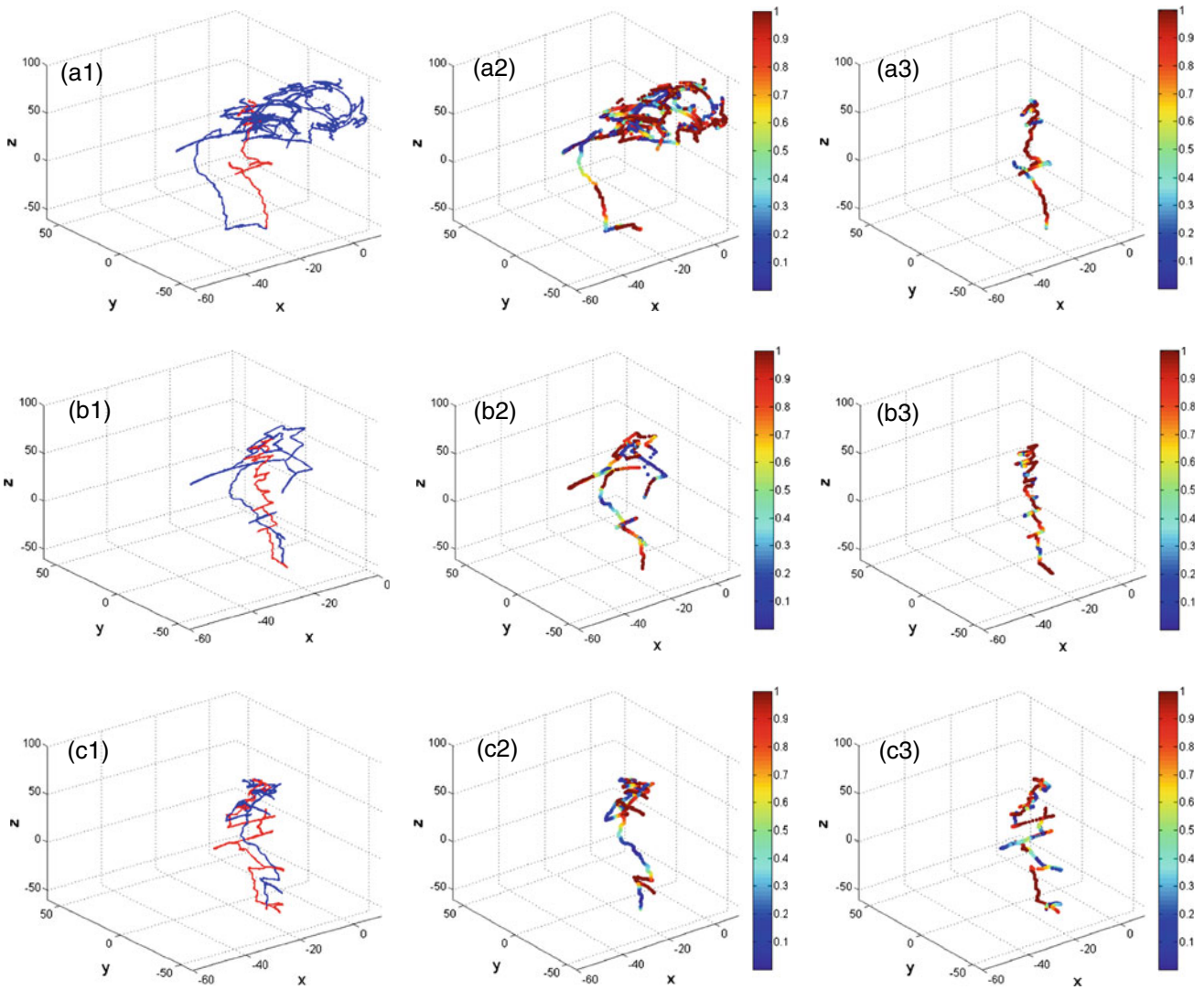

Fig. 6 The catheter tip paths for three operators: **a** operator 4, who improved the most using the reconstructed *frontal view*, **b** operator 6, who improved as most subjects did using the view, and **c** operator 9, who did not improve using the reconstructed *frontal view*. **1** highlights the tip paths with (*red*) and without (*blue*) the reconstructed *frontal view*, **2** shows the tip path without the reconstructed *frontal view* and **3** shows the tip path with the reconstructed *frontal view*, both with the *colourmap* indicating the respiration phase (*0* end inhalation, *1* end exhalation)

Acknowledgments An abstract of this work was presented at the Hamlyn Symposium on Medical Robotics, July 2012, London. The authors wish to thank Mirna Lerotic, Jennifer Keegan, and David Firmin for their assistance with MR data collection.

Conflict of interest Celia Riga, Colin Bicknell and Nicholas Cheshire have Institution level support from Hansen Medical.

References

1. Riga CV, Bicknell CD, Rolls A, Cheshire NJ, Hamady MS (2013) Robot-assisted fenestrated endovascular aneurysm repair (FEVAR) using the Magellan system. J Vasc Interv Radiol 24(2):191–196
2. Chun JK-R, Ernst S, Matthews S, Schmidt B, Bansch D, Boczor S, Ujeyl A, Antz M, Ouyang F, Kuck K-H (2007) Remote-controlled catheter ablation of accessory pathways: results from the magnetic laboratory. Eur Heart J 28(2):190–195
3. Riga CV, Bicknell CD, Hamady MS, Cheshire NJW (2011) Evaluation of robotic endovascular catheters for arch vessel cannulation. J Vasc Surg 54(3):799–809
4. Danilouchkine M, Westenberg J, van Assen H, van Reiber J, Lelieveldt B (2005) 3D model-based approach to lung registration and prediction of respiratory cardiac motion. In: Duncan J, Gerig G (eds) Medical image computing and computer-assisted intervention (MICCAI), Palm Springs, CA, USA. Lecture Notes in Computer Science. Springer, Berlin/Heidelberg, pp 951–959
5. Yang D, Lu W, Low DA, Deasy JO, Hope AJ, Naqa IE (2008) 4D-CT motion estimation using deformable image registration and 5D respiratory motion modeling. Med Phys 35(10): 4577–4590
6. King AP, Rhode KS, Razavi RS, Schaeffter TR (2009) An adaptive and predictive respiratory motion model for image-

guided interventions: theory and first clinical application. IEEE Trans Med Imaging 28(12):2020–2032
7. Kahlert P, Al-Rashid F, Döttger P, Mori K, Plicht B, Wendt D, Bergmann L, Kottenberg E, Schlamann M, Mummel P, Holle D, Thielmann M, Jakob HG, Konorza T, Heusch G, Erbel R, Eggebrecht H (2012) Cerebral embolization during transcatheter aortic valve implantation: a transcranial Doppler study. Circulation 126(10):1245–1255
8. Kesner S, Yuen S, Howe R (2010) Ultrasound servoing of catheters for beating heart valve repair. In: Navab N, Jannin P (eds) Information processing in computer-assisted interventions (IPCAI), Geneva, Switzerland. Lecture Notes in Computer Science. Springer, Berlin/Heidelberg, pp 168–178
9. Deschamps T, Cohen LD (2001) Fast extraction of minimal paths in 3D images and applications to virtual endoscopy. Med Image Anal 5(4):281–299
10. Neubauer A, Wolfsberger S (2013) Virtual endoscopy in neurosurgery: a review. Neurosurgery 72:A97–A106
11. Czarnecka K, Yasufuku K (2012) Interventional pulmonology: focus on pulmonary diagnostics. Respirology 18(1):47–60
12. Sun Z, Lawrence-Brown M (2009) CT virtual endoscopy and 3D stereoscopic visualisation in the evaluation of coronary stenting. Biomed Imaging Intervention J 5(4):e22
13. Sun Z, Chaichana T, Dimpudus FJ, Adipranoto JD, Nugroho J (2009) 3D virtual intravascular endoscopy visualization of coronary artery plaques. In: 3rd international conference on bioinformatics and biomedical engineering (ICBBE), 11–13 June 2009, pp 1–4
14. Wang J, Ohya T, Liao H, Sakuma I, Wang T, Tohnai I, Iwai T (2011) Intravascular catheter navigation using path planning and virtual visual feedback for oral cancer treatment. Int J Med Robotics Comp Assist Surg 7(2):214–224
15. Lee S-L, Chung A, Lerotic M, Hawkins M, Tait D, Yang G-Z (2010) Dynamic shape instantiation for intra-operative guidance. In: Jiang T, Navab N, Pluim J, Viergever M (eds) Medical image computing and computer-assisted intervention (MICCAI), Beijing, China, 2010. Lecture Notes in Computer Science. Springer, Berlin/Heidelberg, pp 69–76
16. Kalman RE (1960) A new approach to linear filtering and prediction problems. Trans ASME J Basic Eng 82(Series D):35–45
17. Lerotic M, Lee S-L, Keegan J, Yang G-Z (2009) Image constrained finite element modelling for real-time surgical simulation and guidance. In: Proceedings of the sixth IEEE international conference on symposium on biomedical imaging: from nano to macro, Boston, Massachusetts, USA, June 28–July 01 2009, pp 1063–1066
18. Lujan AE, Larsen EW, Balter JM, Ten Haken RK (1999) A method for incorporating organ motion due to breathing into 3D dose calculations. Med Phys 26(5):715–720
19. Ganji Y, Janabi-Sharifi F (2009) Catheter kinematics for intracardiac navigation. IEEE Trans Biomed Eng 56(3):621–632
20. Kwok KW, Tsoi KH, Vitiello V, Clark J, Chow GCT, Luk W, Yang GZ (2013) Dimensionality reduction in controlling articulated snake robot for endoscopy under dynamic active constraints. IEEE Trans Robotics Pre-print 99:1–17
21. Riga CV, Cheshire NJW, Hamady MS, Bicknell CD (2007) The role of robotic endovascular catheters in fenestrated stent grafting. J Vasc Surg 51(4):810–820
22. Palágyi K, Kuba A (1999) Directional 3D thinning using 8 subiterations. In: The 8th international conference on discrete geometry for computer imagery, pp 325–336
23. Wang F, Duratti L, Samur E, Spaelter U, Bleuler H (2007) A computer-based real-time simulation of interventional radiology. In: 29th annual international conference of the IEEE engineering in medicine and biology society (EMBS), 22–26 Aug 2007, pp 1742–1745
24. Taylor ZA, Cheng M, Ourselin S (2008) High-speed nonlinear finite element analysis for surgical simulation using graphics processing units. IEEE Trans Med Imaging 27(5):650–663
25. Knight B, Ayers GM, Cohen TJ (2008) Robotic positioning of standard electrophysiology catheters: a novel approach to catheter robotics. J Invasive Cardiol 20(5):250–253
26. Kwok K-W, Mylonas G, Sun L, Lerotic M, Clark J, Athanasiou T, Darzi A, Yang G-Z (2009) Dynamic active constraints for hyper-redundant flexible robots. In: Yang G-Z, Hawkes D, Rueckert D, Noble A, Taylor C (eds) Medical image computing and computer-assisted intervention (MICCAI), London, UK. Lecture Notes in Computer Science. Springer, Berlin/Heidelberg, pp 410–417